

Robotica (2015) volume 33, pp. 209–224. © Cambridge University Press 2014
doi:10.1017/S0263574714000216

Robust tracking of bio-inspired references for a biped robot using geometric algebra and sliding mode control

J. Oviedo-Barriga, L. González-Jiménez,
B. Castillo-Toledo and E. Bayro-Corrochano*

CINVESTAV, Campus Guadalajara, Av. Del Bosque 1145, Col. El Bajío, C.P. 45019, Zapopan, Jalisco, México

(Accepted January 27, 2014. First published online: February 27, 2014)

SUMMARY

Controlling a walking biped robot is a challenging problem due to the robot's complex and uncertain dynamics. In order to tackle this problem, we propose a sliding mode controller based on a dynamic model that we obtained using the conformal geometric algebra (CGA) approach. An important contribution of this paper is the development of algorithms using the CGA framework. The CGA framework permits us to use lines, points, and other geometric entities to obtain the Lagrange equations of the system. The references for the joints of the robot were obtained in a bio-inspired way following the kinematics of a walking human body. The first and second derivatives of the reference signal were obtained via an exact robust differentiator based on a high-order sliding mode. We analyzed the performance of the proposed control schemes by using bio-inspired walking patterns and simulations.

KEYWORDS: Bio-inspired signal; Tracking; Conformal geometric algebra.

1. Introduction

In the area of humanoid robotics, one of the most important issues is dynamic walking control that mimics human-like walking patterns. For the generation and control of such stable and human-like walking by humanoid robots, researchers have proposed various solutions. One of the most widely accepted and used approaches, proposed by Vukobratovic *et al.*¹ in 1970 for generating a reliable hip trajectory for stable biped walking is a walking trajectory based on the zero-moment point (ZMP) stability criterion. With this approach, it is common to define first the ZMP trajectory,^{2–7} and then combine it with the biped's dynamics. The preview controller proposed by Kajita *et al.*,^{2,3} with the idea of previewable optimal control published in 1985, is one such method used to produce a stable hip trajectory. This approach is already used for many types of humanoids to achieve dynamic walking. The main advantage of using this method is its use of the future information about the target signal.⁸ In our work, we focus on the control of bipedal walking. But instead of using a preview control for the generation of walking patterns, we use as reference bio-inspired reference signals. Controlling a bipedal walking robot is a complex task due to several degrees of freedom (DOF), the highly nonlinear dynamics, and a complicated model to describe the behavior of the walking robot. For this reason, we analyze each leg of the biped robot as a serial robotic system and synthesize the dynamic model via the Lagrange equations using the conformal geometric algebra (CGA) approach. A major contribution of this paper is the development of algorithms using the CGA framework. Our work differs from current works because we use the novel CGA framework. The CGA approach allows us to obtain, through a simple procedure, a compact representation of the dynamics of a robotic mechanism. This is due to a simple representation of rigid transformations (rotations, translations, screw motions, etc.) and geometric entities (points, lines, planes, circles, spheres, point pairs, etc.) in this framework.⁹

* Corresponding author. E-mail: edb@gdl.cinvestav.mx

We obtained the references for each joint of the biped robot using the Humanoid Robots Simulation Platform (HRSP), a Simulink toolbox developed by the group of Aleksander Rodic (<http://www.pupin.rs/RnDProfile/robotics/hrsp.html>; <http://www.pupin.rs/RnDProfile/rodic-pub.html>). In addition, the first- and second-order sliding mode controllers were designed to perform tracking of bio-inspired references for biped robot.

Sliding mode control is widely used in uncertain or disturbed systems, featuring robustness and accuracy.¹⁰ An important drawback of the standard sliding mode controller is the presence of high-frequency components in control signals due to the switching function used in its design. In order to attenuate this effect, we use sigmoid functions in the proposed controller as well as a *super-twisting* technique as another solution to reduce high frequencies.^{16,17}

This paper is organized as follows. Section 2 presents a brief introduction to CGA; Section 3 explains the representation of rigid transformations using versors. The dynamic model for the pose of robotic manipulators is obtained in Section 4. The design of the error variables and sliding mode controllers in CGA is presented in Section 5; the structure for the exact robust differentiator is also explained. Section 6 includes an analysis of the application of the designed controllers in a 12-DOF biped robot. Finally, conclusions are given in Section 7.

2. Conformal Geometric Algebra

In order to work in CGA advantageously, we represent the Euclidean vector space \mathbb{R}^3 in the geometric algebra $G_{4,1}$.⁹ This algebra has an orthonormal vector basis given by $\{e_i\}$ and a bivectorial basis defined as $e_{ij} = e_i \wedge e_j$, $e_i \wedge e_\infty$ for $i, j = \{0, 1, 2, 3\}$.

The bivectors e_{23} , e_{31} , and e_{12} correspond to the Hamilton basis, and $E = e_\infty \wedge e_0$ is the Minkowski plane. The unit Euclidean pseudo-scalar $I := e_1 \wedge e_2 \wedge e_3$, and the conformal pseudoscalar $I_c = I_e E$ is used for computing the inverse and duals of multivectors. For more about CGA, see refs. [9, 13].

Let $x_e = [x, y, z]^T$ be a point expressed in \mathbb{R}^3 . The representation of this point in the geometric algebra $G_{4,1}$ is given by

$$x_c = x_e + \frac{1}{2}x_e^2 e_\infty + e_0, \quad (1)$$

where the null vectors are the points at infinity e_∞ and the origin point e_0 , with the properties $e_\infty^2 = e_0^2 = 0$ and $e_\infty \cdot e_0 = 1$.

Given two conformal points x_c and y_c , their difference in Euclidean space can be defined as

$$x_e - y_e = (y_c \wedge x_c) \cdot e_\infty, \quad (2)$$

and, consequently, the following equality

$$(x_c \wedge y_c + y_c \wedge z_c) \cdot e_\infty = (x_c \wedge z_c) \cdot e_\infty \quad (3)$$

is fulfilled, as well.

The line can be obtained in its standard form as

$$L = nI_e - e_\infty mI_e, \quad (4)$$

where n is the orientation and m the moment of the line.

3. Rigid Transformations

These transformations between rigid bodies can be obtained in conformal geometry by carrying out reflections between planes.

3.1. Reflection

A reflection of a point x with respect to a plane π is

$$x' = -\pi x \pi^{-1}, \quad (5)$$

and for any geometric entity Q is

$$Q' = -\pi Q \pi^{-1}. \quad (6)$$

3.2. Translation

The translation can be carried out by two reflections with respect to the parallel planes π_1 and π_2 as

$$Q' = \underbrace{(\pi_2 \pi_1)}_{T_a} Q \underbrace{(\pi_1^{-1} \pi_2^{-1})}_{\tilde{T}_a}, \quad T_a = 1 + \frac{1}{2} a e_\infty = e^{-\frac{a}{2} e_\infty}, \quad (7)$$

with $a = 2dn$, d being the distance of translation, and n the direction of translation.

3.3. Rotation

A rotation is the product of two reflections between the two nonparallel planes π_1 and π_2 that cross the origin. The rotation is then defined by

$$Q' = \underbrace{(\pi_2 \pi_1)}_{R_\theta} Q \underbrace{(\pi_1^{-1} \pi_2^{-1})}_{\tilde{R}_\theta}. \quad (8)$$

Computing the geometric product of the normal of the planes n_1 and n_2 yields

$$\mathbf{R}_\theta = n_2 n_1 = \cos(\theta/2) - \sin(\theta/2) n = e^{-\theta n/2}, \quad (9)$$

with $\mathbf{n} = n_1 \wedge n_2$, and θ is twice the angle between π_1 and π_2 . If we translate the rotor \mathbf{R}_θ to a certain place with the translator $\mathbf{T}_s = 1 + \frac{1}{2} t_s e_\infty$, then the new rotor \mathbf{R} is

$$\mathbf{R} = \mathbf{T}_s \mathbf{R}_\theta \tilde{\mathbf{T}}_s = \cos(\theta/2) - \mathbf{L} \sin(\theta/2), \quad (10)$$

where $\mathbf{L} = \mathbf{n} + e_\infty \mathbf{m}$ is the screw axis, and the bivectors \mathbf{n} and \mathbf{m} stand for the orientation and the moment of the screw axis respectively.

3.4. Screw motion

The screw motion, called motor, is a composition of a translation and a rotation, both related to an arbitrary axis \mathbf{L} . The motor is defined as

$$\mathbf{M} = \mathbf{T} \mathbf{R}. \quad (11)$$

Therefore, a motor transformation for an entity Q is given by

$$Q' = \underbrace{(\mathbf{T} \mathbf{R})}_{M_{\theta,t}} Q \underbrace{(\tilde{\mathbf{R}} \tilde{\mathbf{T}})}_{\tilde{M}_{\theta,t}}. \quad (12)$$

A more detailed description of CGA can be found in ref. [9, 13].

4. Dynamic Modeling Using CGA

Using the equations of kinetic and potential energy as well as the Euler–Lagrange formulation, we may synthesize the dynamic model of any n-DOF serial robot manipulator in terms of CGA.^{12,13} The

matrix form of the Euler–Lagrange equation is given by

$$M(q)\ddot{q} + C(q, \dot{q})\dot{q} + G(q) = \tau. \tag{13}$$

Defining $m_i, I_j, L'_i,$ and x'_i as the mass, moment of inertia, current axis of rotation, and current position of the center of mass for the i th link of the manipulator respectively, we may redefine Eq. (13) in the CGA framework using the following matrices:

$$M(q) = M_v + M_I, \tag{14}$$

where

$$M_I = \delta I = \begin{pmatrix} 1 & 1 & \dots & 1 \\ 0 & 1 & \dots & 1 \\ \vdots & \vdots & \ddots & \vdots \\ 0 & 0 & \dots & 0 \end{pmatrix} \begin{pmatrix} I_1 & 0 & \dots & 0 \\ I_2 & I_2 & \dots & 0 \\ \vdots & \vdots & \ddots & \vdots \\ I_n & I_n & \dots & I_n \end{pmatrix}, \tag{15}$$

and

$$M_v = V^T m V, \tag{16}$$

where $m = \text{diag}\{m_1, m_2, \dots, m_n\}$ and

$$V = \begin{pmatrix} x'_1 \cdot L'_1 & 0 & \dots & 0 \\ x'_2 \cdot L'_1 & x'_2 \cdot L'_2 & \dots & 0 \\ \vdots & \vdots & \ddots & \vdots \\ x'_n \cdot L'_1 & x'_n \cdot L'_2 & \dots & x'_n \cdot L'_n \end{pmatrix}. \tag{17}$$

Based on the properties of the matrices $M(q), C(q, \dot{q})$ as

$$C = V^T m \dot{V}, \tag{18}$$

where

$$V = XL = \begin{pmatrix} x'_1 & 0 & \dots & 0 \\ 0 & x'_2 & \dots & 0 \\ \vdots & \vdots & \ddots & \vdots \\ 0 & 0 & \dots & x'_n \end{pmatrix} \begin{pmatrix} L'_1 & 0 & \dots & 0 \\ L'_1 & L'_2 & \dots & 0 \\ \vdots & \vdots & \ddots & \vdots \\ L'_1 & L'_2 & \dots & L'_n \end{pmatrix}. \tag{19}$$

Therefore,

$$\dot{V} = \dot{X}L + X\dot{L}, \tag{20}$$

where

$$\dot{X} = \begin{pmatrix} \dot{x}'_1 & 0 & \dots & 0 \\ 0 & \dot{x}'_2 & \dots & 0 \\ \vdots & \vdots & \ddots & \vdots \\ 0 & 0 & \dots & \dot{x}'_n \end{pmatrix}, \quad \dot{L} = \begin{pmatrix} \dot{L}'_1 & 0 & \dots & 0 \\ 0 & \dot{L}'_2 & \dots & 0 \\ \vdots & \vdots & \ddots & \vdots \\ 0 & 0 & \dots & \dot{L}'_n \end{pmatrix}. \tag{21}$$

Finally, the vector $G(q)$ is expressed as the following product:

$$G(q) = V^T F, \tag{22}$$

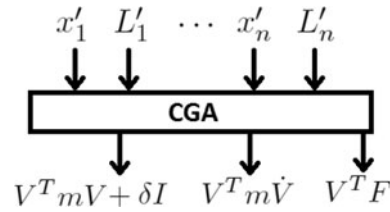


Fig. 1. Measurements for tensors.

with

$$F = \begin{pmatrix} m_1 & 0 & \dots & 0 \\ 0 & m_2 & \dots & 0 \\ \vdots & \vdots & \ddots & \vdots \\ 0 & 0 & \dots & m_n \end{pmatrix} \begin{pmatrix} ge_2 \\ ge_2 \\ ge_2 \\ ge_2 \end{pmatrix}, \tag{23}$$

where g is the acceleration due to gravity. Thus, Eq. (13) will be rewritten as

$$\delta I \ddot{q} + V^T m (V \ddot{q} + \dot{V} \dot{q} + a) = \tau. \tag{24}$$

Note that by using Eq. (24), we obtain the terms using just inner products between X'_i and L'_i . For a more detailed explanation of the process to obtain (13), see Zamora and Bayro-Corrochano.¹³ Using Eq. (24) and measurements of the X'_i and L'_i , we can compute the involved tensor of Eq. (13). In our simulation, we compute these tensors step by step in this way (see Fig. 1).

5. Sliding Mode Controller

In this section, the output tracking problem will be developed for the two legs of a biped robot, each with 6 DOFs, and a sliding mode controller will be proposed.^{14,18} Due to space limitations, we will explain the procedure only for the left leg. Adding a disturbance term $P(t)$ to (13), we can obtain a state-space representation defining the state variables as $x_1 = q$, $x_2 = \dot{q}$, the output of the system as $y = x_1$, and the control signal as $U = \tau$. Hence, the resulting state-space model is given by

$$\begin{aligned} \dot{x}_1 &= x_2, \\ \dot{x}_2 &= -M^{-1} (Cx_2 + G) + M^{-1}U + P(t). \end{aligned} \tag{25}$$

The parentheses were omitted for simplicity and the entries of the tensor were computed using Eq. (24). We assume that the disturbance term $P(t)$ is bounded as follows:

$$\|P(t)\| < \beta. \tag{26}$$

5.1. First-order sliding mode control

Define the output tracking error as

$$e_1 = x_1 - y_{\text{ref}}(t), \tag{27}$$

where y_{ref} is the bio-inspired reference for the biped robot mentioned earlier. Then the dynamics for e_1 is given by

$$\dot{e}_1 = x_2 - \dot{y}_{\text{ref}}(t). \tag{28}$$

Using x_2 as the pseudo-control for this block, we obtain its reference $x_{2\text{ref}}$ as

$$x_{2\text{ref}} = -k_1 \tanh(\varepsilon_1 e_1) + \dot{y}_{\text{ref}}(t). \tag{29}$$

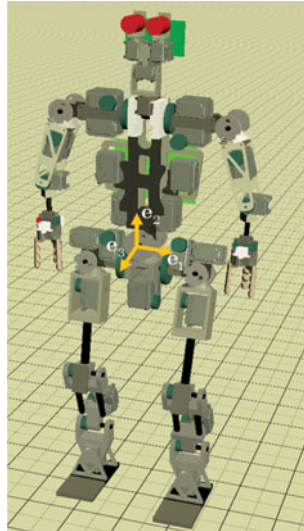


Fig. 2. (Colour online) Biped robot with 6 DOFs per leg.

Then if we define the error variable for the second block as

$$e_2 = x_2 - x_{2\text{ref}}, \quad (30)$$

we can obtain its dynamics as

$$\dot{e}_2 = -M^{-1}(Cx_2 + G) + M^{-1}U + P(t) - \dot{x}_{2\text{ref}}. \quad (31)$$

The term $\dot{x}_{2\text{ref}}$ is defined as

$$\dot{x}_{2\text{ref}} = -k_1 \varepsilon_1 \Phi(x_2 - \dot{y}_{\text{ref}}(t)) + \ddot{y}_{\text{ref}}(t) \quad (32)$$

with $\Phi = \text{diag}\{1 - \tanh^2(\varepsilon_1 e_{11}), \dots, 1 - \tanh^2(\varepsilon_1 e_{1n})\}$ and $e_1 = [e_{11} \dots e_{1n}]^T$.

Finally, we design the control law U as

$$U = Cx_2 + G - k_2 M \text{sgn}(\varepsilon_2 e_2) + M\dot{x}_{2\text{ref}}. \quad (33)$$

Using (33), (31), (29), and (28), we find that the closed-loop dynamics for the error variables is given by

$$\begin{aligned} \dot{e}_1 &= -k_1 \tanh(\varepsilon_1 e_1), \\ \dot{e}_2 &= -k_2 \text{sgn}(\varepsilon_2 e_2) + P(t). \end{aligned} \quad (34)$$

If the conditions $k_1 > 0$, $k_2 > \beta$ are fulfilled, then the system (34) is globally asymptotically stable.¹⁴

A model of the robot humanoid is presented in Fig. 2. It is a 3D virtual representation of the MEXONEexone humanoid robot from CINVESTAV, Campus Guadalajara. Each leg of the biped robot has 6 DOFs: three in the hip, one in the knee, and two in the ankle.

5.2. Second-order sliding mode control

One of the advantages of second-order sliding mode control is that it reduces high-frequency components in the control signal. This technique is known as *super twisting*.^{16,17}

Starting from the state-space model (25), the tracking error e_1 is defined as

$$e_1 = x_1 - y_{\text{ref}}. \quad (35)$$

Then the dynamics for e_1 is given by

$$\dot{e}_1 = x_2 - \dot{y}_{\text{ref}} = -k_1 e_1. \quad (36)$$

Using x_2 as the pseudo-control for this block, we obtain the reference $x_{2\text{ref}}$ as

$$x_{2\text{ref}} = \dot{y}_{\text{ref}} - k_1 e_1. \quad (37)$$

Then the error variable for the second block is defined as

$$e_2 = x_2 - x_{2\text{ref}}. \quad (38)$$

Its dynamics can be obtained as

$$\dot{e}_2 = -M^{-1}(Cx_2 + G) + M^{-1}\tau + P(t) - \dot{x}_{2\text{ref}}, \quad (39)$$

where the control law is proposed as

$$\tau = \tau_0 + \tau_1. \quad (40)$$

τ_0 is the control part that eliminates the known terms of the system, and τ_1 is designed to absorb disturbances. Now (39) can be expressed as

$$\dot{e}_2 = -M^{-1}(Cx_2 + G) + M^{-1}\tau_0 + M^{-1}\tau_1 + P(t) - \dot{x}_{2\text{ref}}, \quad (41)$$

where

$$\tau_0 = (Cx_2 + G) + M\dot{x}_{2\text{ref}}. \quad (42)$$

Then \dot{e}_2 is expressed as

$$\dot{e}_2 = M^{-1}\tau_1 + P(t), \quad (43)$$

and the control τ_1 is proposed as¹⁷

$$\tau_1 = M \left(-k_2 |e_2|^{\frac{1}{2}} \text{sgn}(e_2) + \mu \right), \quad (44)$$

where μ is an auxiliary variable of the super-twisting technique. Finally, (44) is replaced in (43) such that

$$\begin{aligned} \dot{e}_2 &= -k_2 |e_2|^{\frac{1}{2}} \text{sgn}(e_2) + \mu + P(t), \\ \dot{\mu} &= -k_3 \text{sgn}(e_2). \end{aligned} \quad (45)$$

Performing the transformation $\xi = \mu + P(t)$, we obtain

$$\dot{e}_2 = -k_2 |e_2|^{\frac{1}{2}} \text{sign}(e_2) + \xi \quad (46)$$

$$\dot{\xi} = -k_3 \text{sign}(e_2) + \dot{P}(t). \quad (47)$$

5.2.1. Stability. The stability proof was originally done by Moreno *et al.*¹⁷ It is included here for the sake of completeness. The perturbation of the system is globally bounded by

$$|\dot{P}(t)| \leq \delta, \quad (48)$$

where $\delta \geq 0$. The origin is a strong point of equilibrium, globally and asymptotically stable if the gains proposed in ref. [19] satisfy

$$\begin{aligned} k_2 &> 0, \\ k_3 &> 3\delta + 2\frac{\delta^2}{k_2}. \end{aligned} \quad (49)$$

Moreover, all trajectories converge in finite time to the origin, bounded by $\tilde{T} = \frac{2V^{1/2}(x_0)}{\tilde{\gamma}}$, where x_0 is the initial state and $\tilde{\gamma}$ is a constant that depends on the gains k_2, k_3 , and the disturbance coefficient δ . The Lyapunov function for the system (45) is expressed as

$$V = 2k_3 |e_2| + \frac{1}{2} (k_2 |e_2|^{1/2} \operatorname{sgn}(e_2) - \mu)^2. \quad (50)$$

The time derivative of (50) is

$$\dot{V} = -\frac{1}{|e_2|^{1/2}} \zeta^T Q \zeta + \frac{P(t)}{|e_2|^{1/2}} \eta_1^T \zeta, \quad (51)$$

where $\eta_1^T = [(2k_3 + \frac{k_2^2}{2}) - \frac{k_2}{2}]$, $\eta_2^T = [-k_1 \ 2]$, $\zeta^T = [(|e_2|^{1/2} \operatorname{sgn}(e_2)) \ \mu]$, and $Q = \frac{k_2}{2} \begin{bmatrix} 2k_3 + k_2^2 & -k_2 \\ -k_2 & 1 \end{bmatrix}$.

Using the bound on the disturbance (48) and some algebraic manipulation, one can obtain

$$\dot{V} \leq -\frac{1}{|e_2|^{1/2}} \zeta^T \tilde{Q} \zeta, \quad (52)$$

where

$$\tilde{Q} = \frac{k_2}{2} \begin{bmatrix} 2k_3 + k_2^2 - 2\delta - \left(k_2 + \frac{2\delta}{k_2}\right) & \\ -\left(k_2 + \frac{2\delta}{k_2}\right) & 1 \end{bmatrix}. \quad (53)$$

The function (52) is negative definite if $\tilde{Q} > 0$; this is fulfilled under the conditions given in (49). In this way, the state converges to zero in finite time, at most after $T = \frac{2V^{1/2}(x_0)}{\tilde{\gamma}}$ units of time, where $\tilde{\gamma} = \frac{\lambda_{\min}^{1/2}\{\tilde{Q}\}}{\lambda_{\max}\{P\}}$. Taking $e_2 = 0$ in (38), $x_2 = x_{2\text{ref}}$, and $\xi = 0$ in $\xi = \mu + P(t)$, we get $\mu = -P(t)$. Substituting (37) in (36) proves that

$$\dot{e}_1 = -k_1 e_1. \quad (54)$$

Now the Lyapunov function for (54) is

$$V_1 = \frac{1}{2} e_1^T e_1, \quad (55)$$

which is positive definite, and its time derivative is expressed as

$$\begin{aligned} \dot{V}_1 &= e_1^T \dot{e}_1 = e_1^T [-k_1 e_1] = -e_1^T k_1 e_1, \\ &\leq -k_1 \|e_1\|^2. \end{aligned} \quad (56)$$

If the condition $k_1 > 0$ is fulfilled, (56) is negative definite and its origin is a globally and asymptotically stable equilibrium point.

5.3. Exact robust differentiator

In order to implement the control law defined in (33), we need to know the derivatives $\dot{y}_{\text{ref}}(t)$, $\ddot{y}_{\text{ref}}(t)$. Obviously, these are unknown terms because only the reference vector $y_{\text{ref}}(t)$ was obtained by directly

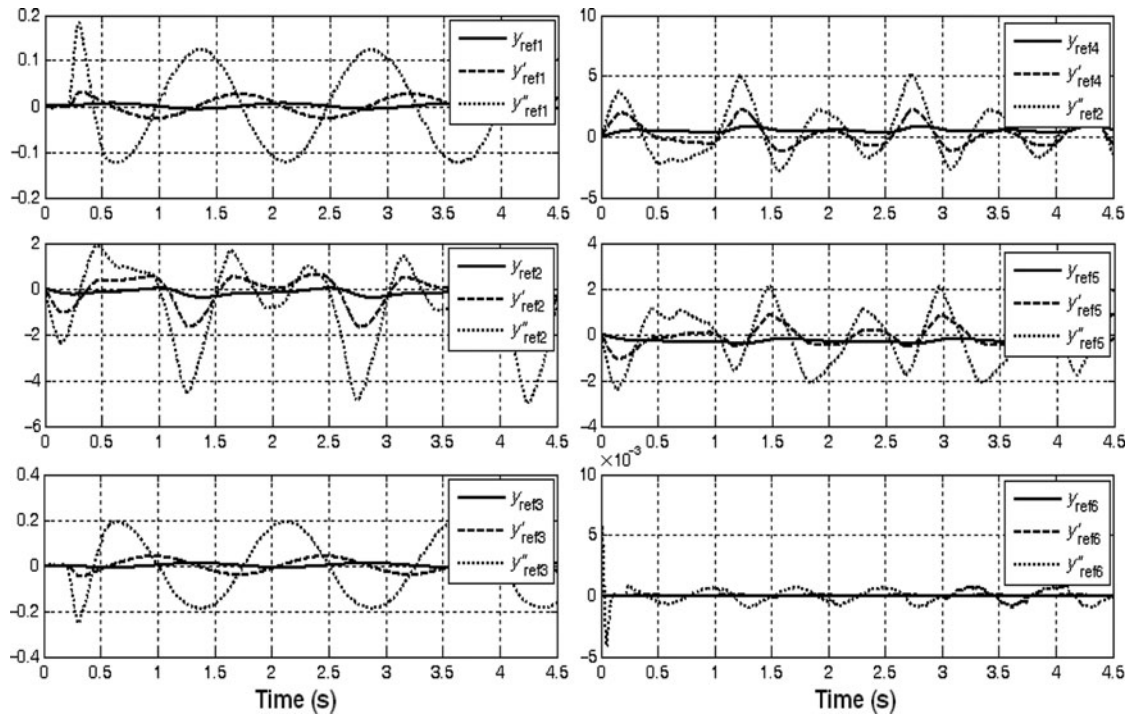


Fig. 3. Reference signal, first derivative, and second derivative for the six joints of the left leg.

measuring a walking person. This missing information can be found using a robust differentiator based on high-order sliding modes.¹⁵ The structure of a fifth-order differentiator is defined as follows:

$$\begin{aligned}
 \dot{z}_0 &= v_0, & v_0 &= -12|z_0 - y_{\text{ref}}(t)|^{5/6} \text{sgn}(z_0 - y_{\text{ref}}(t)) + z_1, \\
 \dot{z}_1 &= v_1, & v_1 &= -8|z_1 - v_0|^{4/5} \text{sgn}(z_1 - v_0) + z_2, \\
 \dot{z}_2 &= v_2, & v_2 &= -5|z_2 - v_1|^{3/4} \text{sgn}(z_2 - v_1) + z_3, \\
 \dot{z}_3 &= v_3, & v_3 &= -3|z_3 - v_2|^{2/3} \text{sgn}(z_3 - v_2) + z_4, \\
 \dot{z}_4 &= v_4, & v_4 &= -1.5|z_4 - v_3|^{1/2} \text{sgn}(z_4 - v_3) + z_5, \\
 \dot{z}_5 &= -1.1 \text{sgn}(z_5 - v_4),
 \end{aligned}
 \tag{57}$$

where z_i is the estimated i th derivative of y_{ref} whose initial value is zero.

Figure 3 shows the bio-inspired walking references for the six joints of the left leg and the output of the robust differentiator for the first and second derivatives. Note that the references for each joint of the biped robot were obtained using the HRSP, where reference signals at each joint of a walking person (human) are captured using the VICON system. The signals are adapted via fuzzy logic and neural network-based inference engine, taking into account the gait and parameter characteristics of the 106-cm tall humanoid MEXONE.

The walking process of a biped robot includes the swing and the collision phase when the feet touch the floor. In this study, our walking patterns show a smooth transition between phases; thus, the control algorithms applied to dynamic equations adapt smoothly to the system. However, due to the use of the super-twisting sliding mode control, which is robust against unmatched perturbations, the biped robot will indeed maintain its smooth walking even under these perturbations.

Figure 4 shows the bio-inspired signals for each joint of the legs.

6. Simulations

The proposed control law defined in (33) was applied to the biped robot shown in Fig. 2. The axes of rotation are proposed in Fig. 5. The initial value of the vector for both legs is $x_0 = 10^{-2} \cdot [5 \ 21 \ 8 \ 62 \ 15 \ 0.003]^T$, and the gains k_1, k_2 were set as $k_1 = 10 \cdot [1 \ 4 \ 1 \ 4 \ 4 \ 2]^T$ and $k_2 = 10 \cdot$

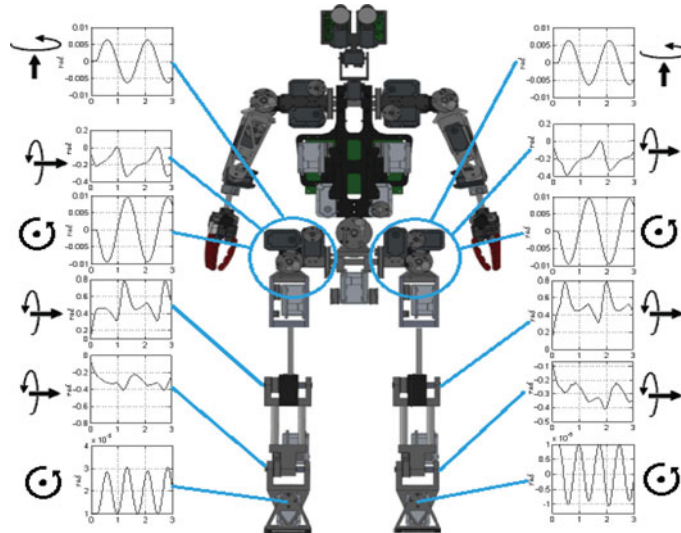


Fig. 4. (Colour online) Bio-inspired reference signals for the joints of each leg.

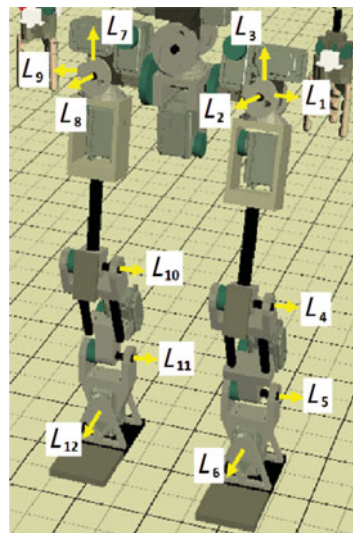


Fig. 5. (Colour online) Axes of rotation of the biped robot.

$[1 \ 28 \ 1 \ 28 \ 14 \ 4]^T$ respectively. The slopes $\varepsilon_1, \varepsilon_2$ were chosen as $\varepsilon_1 = 2, \varepsilon_2 = 5$. The initial positions for the center of mass of each link are

$$\begin{aligned}
 x_1 &= \sigma_1 e_1 - \sigma_2 e_2, & x_7 &= -\sigma_1 e_1 - \sigma_2 e_2, \\
 x_2 &= \sigma_3 e_1 - \sigma_2 e_2, & x_8 &= -\sigma_3 e_1 - \sigma_2 e_2, \\
 x_3 &= \sigma_4 e_1 - \sigma_5 e_2, & x_9 &= -\sigma_4 e_1 - \sigma_5 e_2, \\
 x_4 &= \sigma_4 e_1 - \sigma_6 e_2, & x_{10} &= -\sigma_4 e_1 - \sigma_6 e_2, \\
 x_5 &= \sigma_4 e_1 - \sigma_7 e_2, & x_{11} &= -\sigma_4 e_1 - \sigma_7 e_2, \\
 x_6 &= \sigma_4 e_1 - \sigma_8 e_2, & x_{12} &= -\sigma_4 e_1 - \sigma_8 e_2,
 \end{aligned} \tag{58}$$

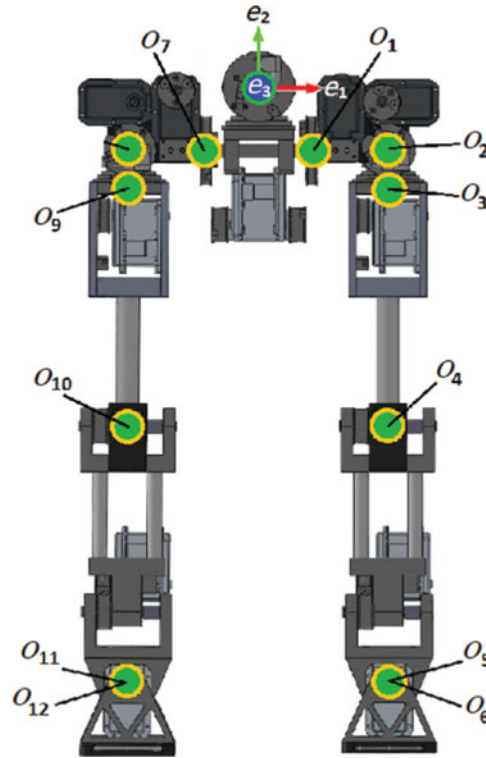


Fig. 6. (Colour online) Origins of the frames attached to each link.

and the origins of the frames attached to each link of the biped robot are the following Euclidean points, which can be expressed in CGA using Eq. (1) as follows:

$$\begin{aligned}
 o_1 &= \sigma_9 e_1 - \sigma_2 e_2, & o_7 &= -\sigma_9 e_1 - \sigma_2 e_2, \\
 o_2 &= \sigma_4 e_1 - \sigma_2 e_2, & o_8 &= -\sigma_4 e_1 - \sigma_2 e_2, \\
 o_3 &= \sigma_4 e_1 - \sigma_3 e_2, & o_9 &= -\sigma_4 e_1 - \sigma_3 e_2, \\
 o_4 &= \sigma_4 e_1 - \sigma_{10} e_2, & o_{10} &= -\sigma_4 e_1 - \sigma_{10} e_2, \\
 o_5 &= \sigma_4 e_1 - \sigma_8 e_2 = o_6, & o_{11} &= -\sigma_4 e_1 - \sigma_8 e_2 = o_{12},
 \end{aligned} \tag{59}$$

with $\sigma_1 = 0.024$, $\sigma_2 = 0.062$, $\sigma_3 = 0.079$, $\sigma_4 = 0.110$, $\sigma_5 = 0.068$, $\sigma_6 = 0.188$, $\sigma_7 = 0.417$, $\sigma_8 = 0.533$, $\sigma_9 = 0.049$, and $\sigma_{10} = 0.302$, all of which depend on the magnitude of the distances between the reference frame $\{e_1, e_2, e_3\}$ and the origins o_i , $i = 1, \dots, 12$, indicated in Fig. 6. The initial values for the axes of rotation of the biped robot are defined as

$$\begin{aligned}
 L_1 &= e_{23} + e_\infty(o_1 \cdot e_{23}), & L_7 &= e_{23} + e_\infty(o_7 \cdot e_{23}), \\
 L_2 &= e_{12} + e_\infty(o_2 \cdot e_{12}), & L_8 &= e_{12} + e_\infty(o_8 \cdot e_{12}), \\
 L_3 &= e_{31} + e_\infty(o_3 \cdot e_{31}), & L_9 &= e_{31} + e_\infty(o_9 \cdot e_{31}), \\
 L_4 &= e_{23} + e_\infty(o_4 \cdot e_{23}), & L_{10} &= e_{23} + e_\infty(o_{10} \cdot e_{23}), \\
 L_5 &= e_{23} + e_\infty(o_5 \cdot e_{23}), & L_{11} &= e_{23} + e_\infty(o_{11} \cdot e_{23}), \\
 L_6 &= e_{12} + e_\infty(o_6 \cdot e_{12}), & L_{12} &= e_{12} + e_\infty(o_{12} \cdot e_{12}).
 \end{aligned} \tag{60}$$

The simulation results for the left leg are shown next. The performance and response for the right leg are very similar to the left leg and thus are not included here. The disturbance signals used in the simulation can be seen in Fig. 7.

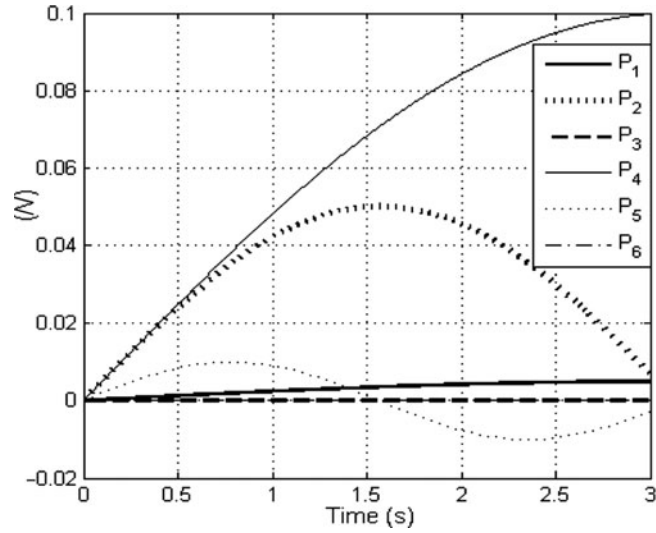


Fig. 7. Disturbances used in the simulation for each joint of the left leg.

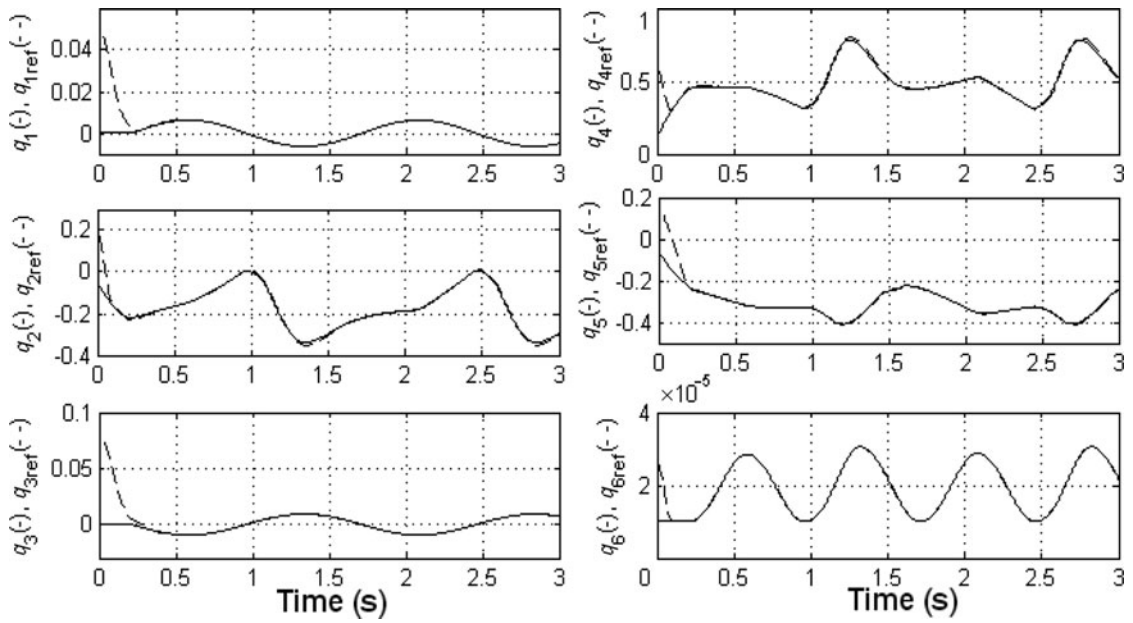


Fig. 8. Tracking response for the six joints of the left leg (first-order sliding mode control).

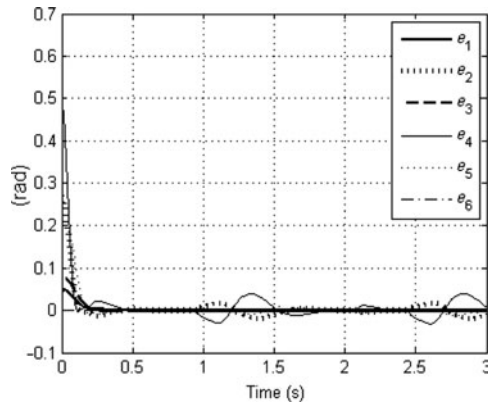


Fig. 9. Tracking error for the six joints of the left leg (first-order sliding mode control).

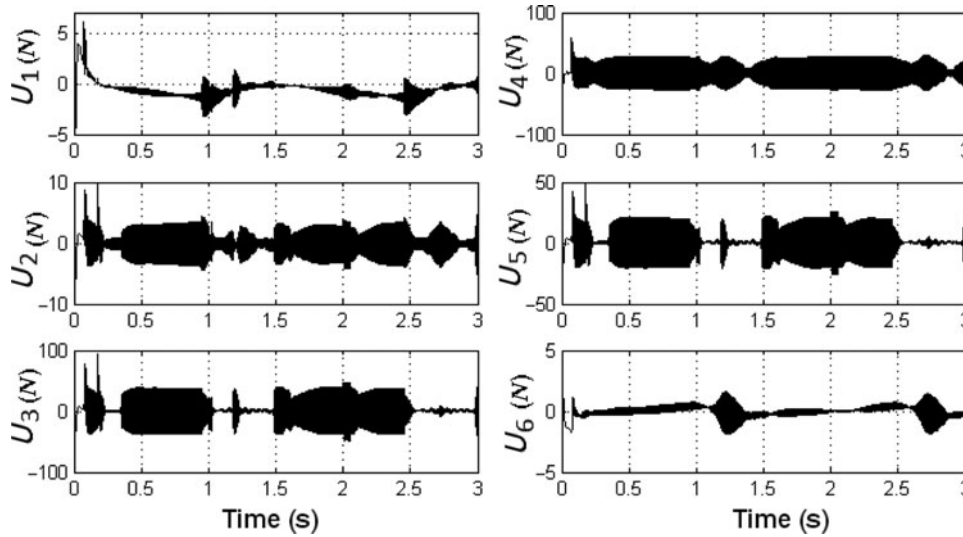


Fig. 10. Control signals (joint torques) for the six joints of the left leg (first-order sliding mode control).

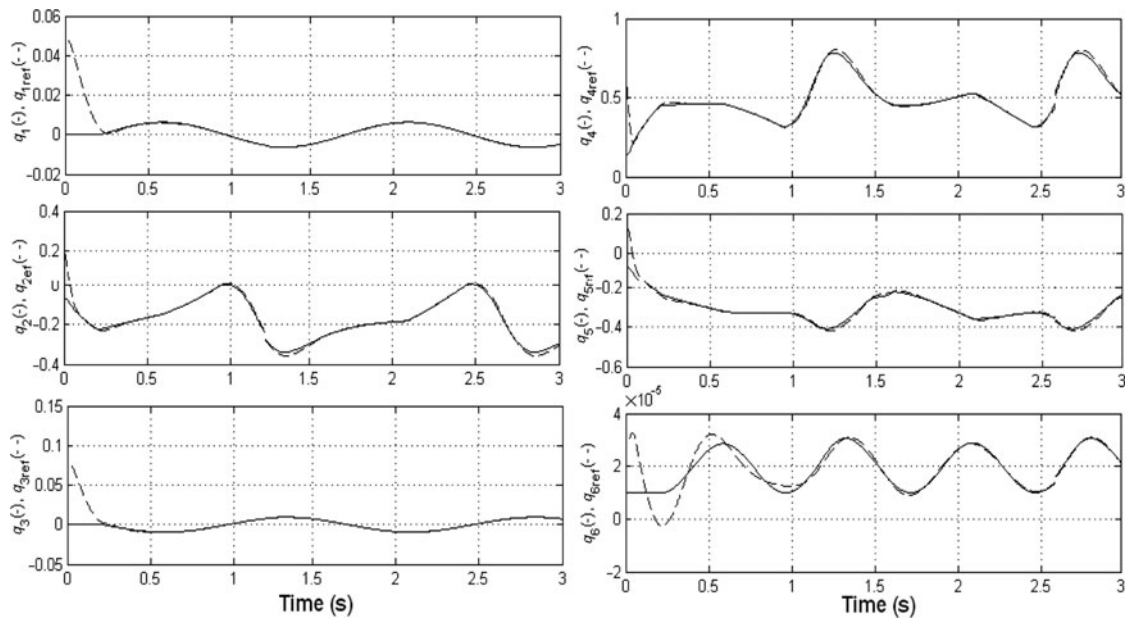


Fig. 11. Tracking response for the six joints of the left leg (super-twisting technique).

6.1. Simulations using first-order sliding mode control

The tracking responses for the six joints of the left leg are depicted in Fig. 8. One can observe that the control objective has been fulfilled, and with a low settling time. Figure 9 shows that the six corresponding error variables converge to a small vicinity of zero, demonstrating the robustness of the proposed control scheme. Figure 10 depicts the control signals (joint torques) of the left leg.

6.2. Simulations using the super-twisting technique

The tracking responses for the six joints of the left leg are depicted in Fig. 11. One can observe that the control objective has been fulfilled, and with a low settling time. Figure 12 shows that the six corresponding error variables converge to a smaller vicinity of zero using the super-twisting technique. Note that this vicinity is smaller than that using first-order sliding mode control, thus demonstrating the robustness of the super-twisting control technique. In addition, we show how the chattering is almost eliminated with the super-twisting control technique. This capability is very useful in order not to damage the actuators of a real robot. In Fig. 13, the control signals (joints torques) of the left

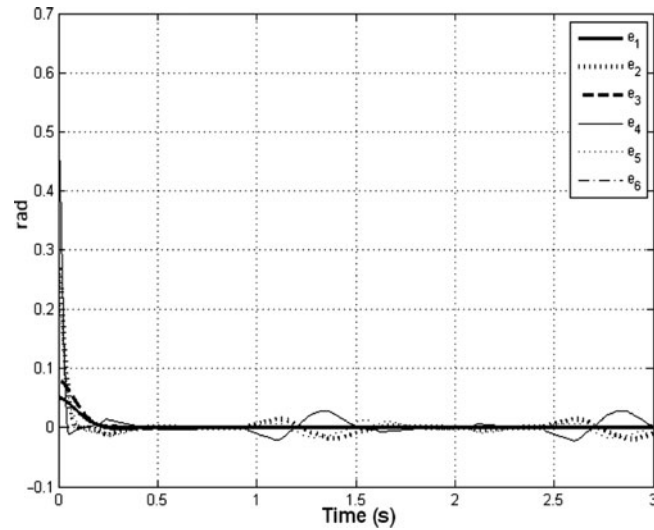


Fig. 12. Tracking error for the six joints of the left leg (super-twisting technique).

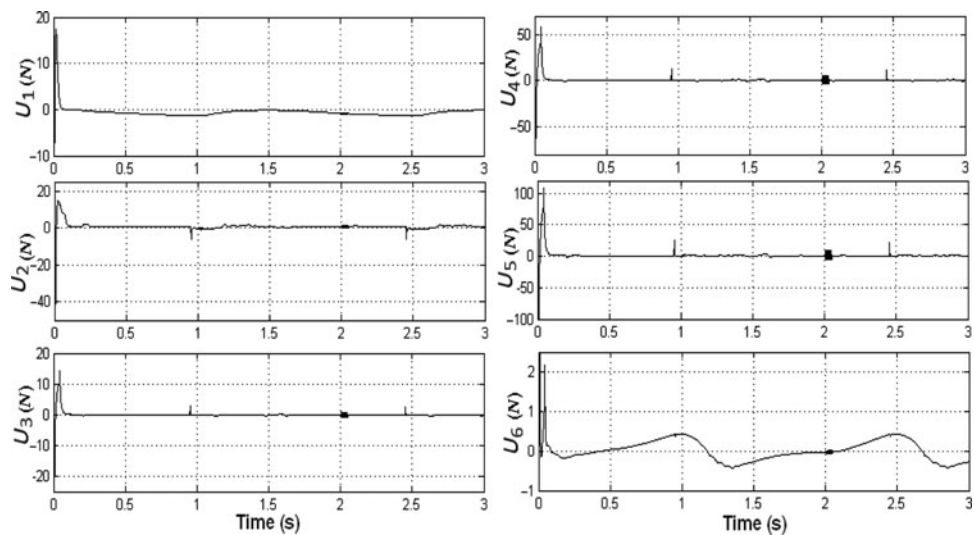


Fig. 13. Control signals (joint torques) for the six joints of the left leg (super-twisting technique).

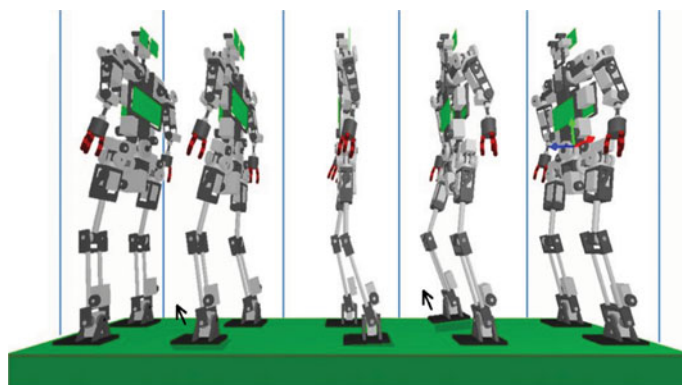


Fig. 14. (Colour online) Sequence of images of the biped robot walking (two steps). The arrows indicate the feet lifting.

leg are depicted using the super-twisting technique. The high-frequency components are significantly attenuated, unlike in Fig. 10, even though the setting time is a bit longer than the control schema using first-order sliding mode control. Finally, a sequence of images of the biped robot walking is presented in Fig. 14. In future work, we will use a series of tracking-control analyses based on different gait characteristic data following more challenging walking paths and under lateral pushing. We will soon apply these control techniques with our robot in real time.

7. Conclusions

We applied bio-inspired signals as walking waves as reference for the walking of a humanoid robot. The advantage of using such signals is that they help us to get the robot to accomplish an expected human-like walking pattern. However, this is jeopardized due to the effect of perturbations and non-modeled parameters of the robot dynamics. To follow such trajectories, we must resort to a robust control technique. In addition, the algebraic complexity of the formulation is also an issue, which we tackle by computing the kinematics and dynamics of the plant in the CGA framework. As a result, the equations are simple, compact, and comfortable for design algorithms subject to geometric constraints. In this regard, the use of a robust sliding mode controller becomes easy and natural. We present simulations subject to perturbations that confirm the robustness of our control schemes. Future work consists of using more advanced control techniques and real-time implementation.

Acknowledgment

This work was supported in part by PhD scholarship no. 28824.

References

1. M. Vukobratovic and B. Borovac, "Zero-moment point thirty five years of its life," *Int. J. Humanoid Robot.* **1**(1), 157–173 (2004).
2. S. Kajita, F. Kanehiro, K. Kaneko, K. Fujiwara, K. Harada, K. Yokoi and H. Hirukawa, "Biped Walking Pattern Generation by Using Preview Control of Zero-Moment Point," *Proceedings of the IEEE International Conference on Robotics and Automation (ICRA 2003)*, vol. 2 (2003) pp. 1620–1626.
3. S. Kajita, F. Kanehiro, K. Kaneko, K. Yokoi and H. Hirukawa, "The 3D Linear Inverted Pendulum Mode: A Simple Modeling for a Biped Walking Pattern Generation," *Proceedings of the 2001 IEEE/RSJ International Conference on Intelligent Robots and Systems (IROS 2001)*, vol. 1 (2001) pp. 239–246.
4. Y. Choi, B.-J. You and S.-R. Oh, "On the Stability of Indirect ZMP Controller for Biped Robot Systems," *Proceedings of the 2004 IEEE/RSJ International Conference on Intelligent Robots and Systems (IROS 2004)*, vol. 2 (2004) pp. 1966–1971.
5. J. Park and Y. Youm, "General ZMP Preview Control for Bipedal Walking," *Proceedings of the 2007 IEEE International Conference on Robotics and Automation (ICRA 2007)* (2007) pp. 2682–2687.
6. K.-K. Noh, J.-G. Kim and U.-Y. Huh, "Stability Experiment of a Biped Walking Robot with Inverted Pendulum," *Proceedings of the 30th Annual Conference of IEEE Industrial Electronics Society (IECON 2004)*, vol. 3 (2004) pp. 2475–2479.
7. I.-W. Park, J.-Y. Kim and J.-H. Oh, "Online Biped Walking Pattern Generation for Humanoid Robot KHR-3 (KAIST Humanoid Robot-3: HUBO)," *Proceedings of the 6th IEEE-RAS International Conference on Humanoid Robots (Humanoids 2006)* (2006) pp. 398–403.
8. T. Katayama, T. Ohki, T. Inoue and T. Kato, "Design of an optimal controller for a discrete-time system subject to previewable demand," *Int. J. Control* **41**(3), 677–699 (1985).
9. E. Bayro-Corrochano, *Geometric Computing: For Wavelet Transforms, Robot Vision, Learning, Control and Action* (Springer, London, 2010).
10. V. I. Utkin, J. Guldner and J. Shi, *Sliding Mode Control in Electromechanical Systems* (Taylor and Francis, Boca Raton, FL, 1999).
11. H. Li, D. Hestenes and A. Rockwood, "Generalized Homogeneous Coordinates for Computational Geometry," **In: Geometric Computing with Clifford Algebras** (G. Somer, ed.) (Springer-Verlag, Heidelberg, Germany, 2001) pp. 27–52.
12. J. Zamora and E. Bayro-Corrochano, "Kinematics and Differential Kinematics of Binocular Heads," *Proceedings of the International Conference of Robotics and Automation (ICRA 2006)*, Orlando, FL (2006) pp. 4130–4135.
13. J. Zamora and E. Bayro-Corrochano, "Parallel Forward Dynamics: A Geometric Approach," *Proceedings of the International Conference on Intelligent Robots and Systems (IROS 2010)*, Taiwan (2010) pp. 18–22.

14. L. González-Jiménez, A. Loukianov and E. Bayro-Corrochano, "Integral Nested Sliding Mode Control for Robotic Manipulators," *Proceedings of the 17th World Congress of the International Federation of Automatic Control*, Seoul, Korea (2008) pp. 9899–9904.
15. A. Levant, "Higher order modes, differentiation and output feedback control," *Int. J. Control* **76**, 924–941 (2003).
16. A. Levant, "Sliding order and sliding accuracy in sliding mode control," *Int. J. Control* **58**, 1247–1263 (1993).
17. J. A. Moreno and M. Osorio "A Lyapunov Approach to Second-Order Sliding Mode Controllers and Observers," *Proceedings of the 47th Conference on Decision and Control*, Cancún, México (Dec. 9–11, 2008) pp. 2856–2861.
18. J. Oviedo-Barriga, O. Carbajal-Espinosa, L. González-Jiménez, B. Castillo-Toledo and E. Bayro-Corrochano, "Robust Tracking of Bio-Inspired References for a Biped Robot Using Geometric Algebra and Sliding Mode," *Proceedings of the IEEE International Conference on Robotics and Automation (ICRA 2013)*, Karlsruhe, Germany (May 6–10, 2013) pp. 5297–5302.